A Modeling of Buoyant Gas Plume Migration

Dmitriy Silin
Lawrence Berkeley National Laboratory, 1 Cyclotron Road, MS 90-1116, Berkeley, CA 94720, USA

Tad W. Patzek
University of California, Berkeley, 425 Davis Hall, Berkeley, CA 94720, USA

Sally M. Benson
Energy Resources Engineering Department, Stanford University, 074 Green Sciences Building, 367 Panama Street, Stanford, CA 94305-22020, USA

Abstract

This work is motivated by the growing interest in injecting carbon dioxide into deep geological formations as a means of avoiding its atmospheric emissions and consequent global warming. Ideally, the injected greenhouse gas stays in the injection zone for a geologic time, eventually dissolves in the formation brine and remains trapped by mineralization. However, one of the potential problems associated with the geologic method of sequestration is that naturally present or inadvertently created conduits in the cap rock may result in a gas leakage from primary storage. Even in a supercritical state, the carbon dioxide viscosity and density are lower than

those of the formation brine. Buoyancy tends to drive the leaked CO_2 plume upward. Theoretical and experimental studies of buoyancy-driven supercritical CO_2 flow, including estimation of time scales associated with plume evolution and migration, are critical for developing technology, monitoring policy, and regulations for safe carbon dioxide geologic sequestration.

In this study, we obtain simple estimates of vertical plume propagation velocity taking into account the density and viscosity contrast between CO_2 and brine. We describe buoyancy-driven countercurrent flow of two immiscible phases by a Buckley-Leverett type model. The model predicts that a plume of supercritical carbon dioxide in a homogeneous water-saturated porous medium does not migrate upward like a bubble in bulk water. Rather, it spreads upward until it reaches a seal or until it becomes immobile. A simple formula requiring no complex numerical calculations describes the velocity of plume propagation. This solution is a simplification of a more comprehensive theory of countercurrent plume migration (Silin et al., 2007). In a layered reservoir, the simplified solution predicts a slower plume front propagation relative to a homogeneous formation with the same harmonic mean permeability. In contrast, the model yields much higher plume propagation estimates in a high-permeability conduit like a vertical fracture.

Key words: geologic sequestration, buoyancy, countercurrent flow, plume migration

---

* Corresponding author.
Email addresses: DSilin@lbl.gov (Dmitriy Silin), patzek@patzek.berkeley.edu (Tad W. Patzek), SMBenson@stanford.edu (Sally M. Benson).

1 Introduction

This work is motivated by the growing interest in injecting carbon dioxide into deep geological formations as a means of avoiding its atmospheric emissions and consequent global warming. Ideally, the injected gas stays in the injection zone for a long time, is dissolved in the formation brine, and becomes trapped by mineralization. However, a gas leakage from primary storage may occur because of cracks or other naturally or inadvertently man-made conduits in the cap rock. Even if the injected carbon dioxide is in supercritical state, its viscosity and density are lower than those of the *in situ* formation brine. Therefore, buoyancy always drives the injected carbon dioxide upward. Understanding the buoyancy-driven plume migration and estimation of the time scales associated with plume evolution are critical for developing appropriate regulations protecting safety of potable water resources.

The objective of this study is to characterize the evolution of a plume of supercritical carbon dioxide in a water-saturated porous medium. The model is one-dimensional, which means that we focus of the evolution of a horizontally-spread plume far from its lateral boundaries. We estimate the velocity of plume propagation taking into account the density and viscosity contrast between the injected CO_2 and formation water. This work follows previous studies (Silin et al., 2006, 2007) where a more general model of two-phase vertical counter-current flow has been discussed. Here, we simplify that model by neglecting capillary forces. This simplification leads to a more transparent theory while preserving the main conclusion of the more general approach. Two-phase flow is characterized by a hyperbolic equation, which is then solved using method of characteristics (Petrovskii, 1966; Lax, 1973). Mathematically, the evolution

of the plume is described as a sequence of exact solutions usually called shock and rarefaction waves. The theory then predicts that in a porous medium, the plume does not migrate upward like a gas bubble in bulk water. Rather, the gas spreads upward until it hits a seal or reaches a uniform immobile gas saturation. The simplified model discussed here predicts the same plume propagation velocity estimates as the model studied by Silin et al. (2007).

The hyperbolic flow model can be easily extended to characterize propagation of the front of the plume through a layered aquifer. The theory predicts that a low-permeability layer significantly reduces the speed of propagation in all overlaying strata. If the heterogeneity of the medium includes a conductive vertical fracture, the plume propagation inside the fracture is much faster than in the rest of the formation.

Section 2 briefly overviews an extension of the Buckley–Leverett hyperbolic model to a buoyancy-driven two-phase countercurrent flow. Section 3 discusses typical solutions and their physical interpretations, both for homogeneous and heterogeneous formations. Conclusions and recommendations are summarized in sections 4 and 5. For brevity, the injected supercritical carbon dioxide will be called gas.

2 The model

A carbon dioxide plume migration involves various complex processes acting in different time scales. Juanes et al. (2006) formulate five principal mechanisms of CO_2 trapping: hydrodynamic trapping, solution trapping, mineral trapping, capillary trapping, and two-phase flow hysteresis. The latter is a consequence

of gas trapping by water imbibing in water-wet rocks (Al-Futaisi and Patzek, 2003; Valvante and Blunt, 2004).

In this work, we focus on the buoyancy-driven two-phase viscous flow. In the literature, somewhat similar two-phase flow models have been considered in the context of secondary hydrocarbon migration (Luan, 1994; Siddique and Lake, 1997; Bedrikovetsky et al., 2001). Our choice is based on the assumption that near the front of the plume dissolution and geochemistry are much slower than the flow. In addition, if a leaking plume loses carbon dioxide at a certain rate as it migrates under buoyancy, such losses can only slow down the plume propagation. Thus, the estimates obtained here can be qualified as the worst-case scenario.

2.1 Buckley–Leverett model of two-phase flow

Assume that the carbon dioxide plume crosses a thick aquifer with uniform flow properties. Let the vertical coordinate, z, be directed upward. Thus, a positive Darcy velocity means upward flow. Darcy's law for two-phase flow states the following relationships between the Darcy velocities of gas and brine and their respective pressure gradients (Muskat, 1949; Hubbert, 1956):

$$u_g = -\frac{k_{rg}(S)k}{\mu_g}\left(\frac{\partial p_g}{\partial z} - \varrho_g g\right) \tag{1}$$

$$u_w = -\frac{k_{rw}(S)k}{\mu_w}\left(\frac{\partial p_w}{\partial z} - \varrho_w g\right) \tag{2}$$

Here u_g and u_w are the Darcy velocities, or volumetric fluxes, of the gas and liquid, μ_g and μ_w are their dynamic viscosities, p_g and p_w, and ϱ_g and ϱ_w are their pressures and densities, respectively. Volumetric saturation of the brine and gravity acceleration are denoted by S and g, and k is the absolute

permeability of the medium. In this derivation, we neglect the compressibility of brine and supercritical gas. Since there is no sink or source of gas or brine, the flow is countercurrent:

$$u_g + u_w = 0 \tag{3}$$

To obtain equations in dimensionless form, we introduce a dimensionless vertical coordinate ζ and time τ:

$$\zeta = \frac{z}{H} \qquad \tau = \frac{k\,(\varrho_w - \varrho_g)\,g}{\mu_w H}\,t \tag{4}$$

Here H is the thickness of the reservoir. In what follows, we assume that the following condition holds true:

$$\left|\gamma \mathcal{J}'(S)\frac{\partial S}{\partial \zeta}\right| \ll 1 \tag{5}$$

where $\mathcal{J}$ is Leverett's J-function (Leverett et al., 1942) and

$$\gamma = \frac{\sigma}{(\varrho_w - \varrho_g)gH}\sqrt{\frac{\phi}{k}} \tag{6}$$

is an analog of the reciprocal Bond number. Under assumption (5), the impact of capillarity is negligible (Silin et al., 2006).

Combination of Darcy's law with the mass balance yields a hyperbolic equation for brine saturation S:

$$\phi\frac{\partial S}{\partial \tau} - \frac{\partial}{\partial \zeta}f(S) = 0 \tag{7}$$

where

$$f(S) = \frac{k_{rw}(S)}{\dfrac{k_{rw}(S)}{k_{rg}(S)}\dfrac{\mu_g}{\mu_w} + 1} \tag{8}$$

Equation (7) constitutes a Buckley–Leverett type flow model (Buckley and Leverett, 1942) in dimensionless form. The dimensionless Darcy velocity of

the brine,

$$W_w = \frac{\mu_w}{k(\varrho_w - \varrho_g)g} u_w \tag{9}$$

equals minus fractional flow function:

$$W_w = -f(S) \tag{10}$$

2.2 Shock and rarefaction wave solutions

A solution to the hyperbolic equation (7) propagates along characteristics (Petrovskii, 1966; Lax, 1973). The theory predicts two types of stable saturation profiles. Using the terminology of gas dynamics (Landau and Lifshitz, 1959), such profiles are called shock and rarefaction waves. In the model under consideration, a solution of the first type characterizes an abrupt variation of the saturation profile. The second one characterizes a stretching smooth saturation profile.

Consider a shock wave. If S_1 and S_2 denote the saturations ahead and behind the front, then mass balance yields the following expression for the dimensionless shock propagation velocity:

$$V_s(S_1, S_2) = -\frac{1}{\phi} \frac{f(S_2) - f(S_1)}{S_2 - S_1} \tag{11}$$

Note that the expression on the right-hand side can be either positive or negative, or be equal to zero for an equilibrium saturation transition.

A rarefaction-wave saturation profile is provided by the implicit relationship

$$\zeta = \zeta_0 - \tau \frac{1}{\phi} f'\left(S(\tau, \zeta)\right) \tag{12}$$

where ζ_0 is the initial location of the center of the wave. Equation

$$V_r(S) = -\frac{1}{\phi} f'(S) \tag{13}$$

expresses the velocity of propagation of the part of the rarefaction wave, where the brine saturation is equal to S. If a shock wave with saturations S_1 and S_2 before and behind the front is followed or preceded by a rarefaction wave, then mass balance implies

$$f'(S_i) = \frac{f(S_2) - f(S_1)}{S_2 - S_1} \tag{14}$$

where i is either 1 or 2.

3 Results and Discussion

We begin with describing evolution of the plume in a homogeneous formation as a sequence of shock and rarefaction waves. The theory of two-phase buoyancy-driven flow predicts that the main part of the plume is almost stationary, being reduced from the top by the leading propagating front. Evolution of this leading front is much faster that the evolution of the rest of the plume. The leading part of the plume is relatively lean with respect to gas saturation. For simplicity, we consider an initial plume with a constant gas saturation. We put the origin $z = 0$ at the top of the initial plume (Figure 1). In calculations, we use van Genuchten parametrization of relative permeability curves with parameter values used by Xu et al. (2005).

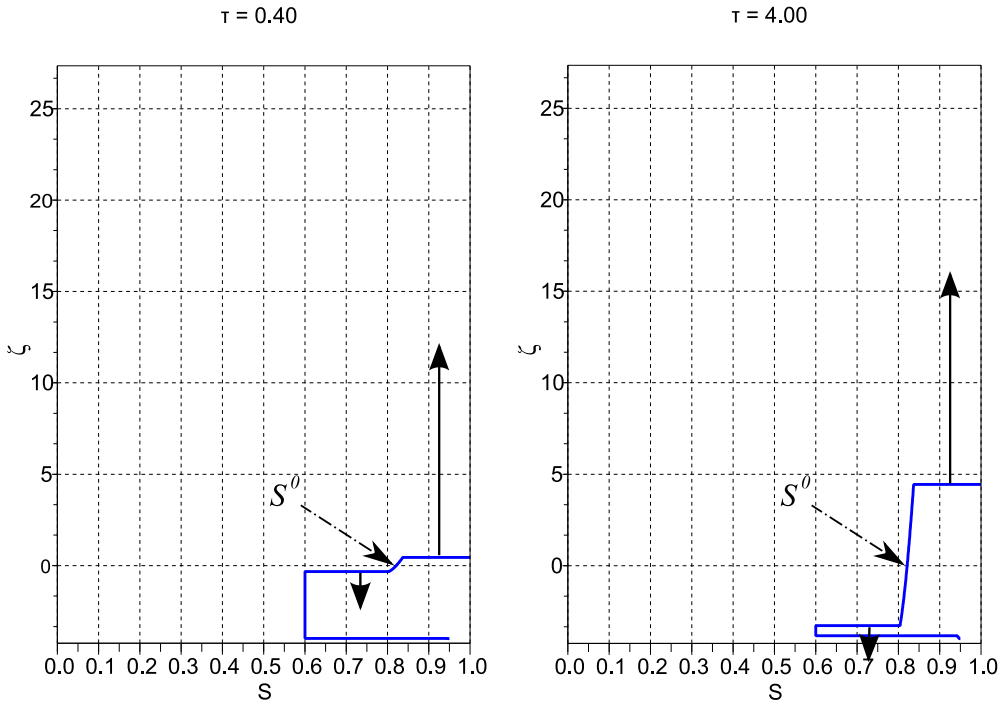

Fig. 1. Vertical brine saturation profile in dimensionless coordinates at an early stage of plume evolution. The initial saturation of gas is 40 %. A leading front of low gas saturation propagates upward, whereas the main part of the plume gradually shrinks. The arrows show the directions of propagation of the fronts. Here $S_0 = S(\zeta = 0)$

3.1 The leading front of the plume

In estimating the plume propagation time, the most critical part is the top leading front of the plume. Assuming that the formation ahead of the plume is entirely saturated by brine and saturation of the brine behind the front is denoted by S^*, Equations (4) and (11) imply that the dimensionless front propagation velocity is equal

$$V^* = \frac{1}{\phi}\frac{f(S^*)}{1 - S^*} \tag{15}$$

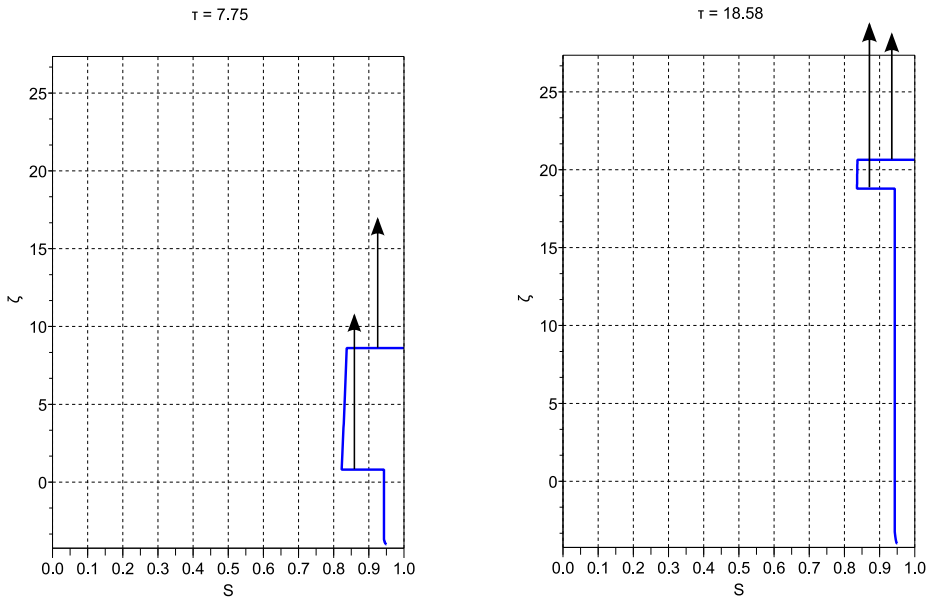

Fig. 2. Evolution of the plume after its main part collapses. The lean leading part of the plume migrates upward whereas gas saturation behind it approaches the residual saturation.

In physical units,

$$v^* = \frac{k(\varrho_w - \varrho_g)g}{\phi\mu_w}\frac{f(S^*)}{1-S^*} \tag{16}$$

Front stability analysis suggests that the expression on the right-hand side of Equation (15) attains its maximum at $S = S^*$.

3.2 Evolution of the main part of the plume

The evolution of the saturation profile behind the leading part of the plume described in the previous section can be characterized as a sequence of two rarefaction and two shock waves. Figures 1–3 display the profiles at different times in dimensionless units. The theory predicts three stages of plume evolution. At early time, the high-gas-saturation part of the plume thins between two traveling shock waves in the saturation profile propagating in the opposite

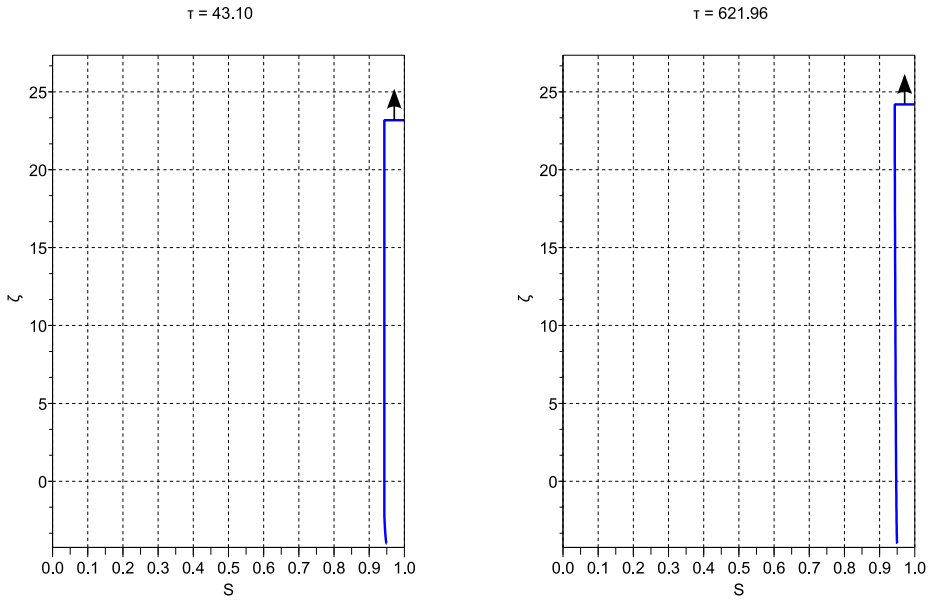

Fig. 3. The final phase of plume evolution. The bottom rarefaction wave characterizes the saturation profile in most of the plume. The gas is close to being trapped over the entire plume.

directions (Figure 1). At the top, a travelling wave propagates downward to compensate for the flow of gas in the leading part. At the bottom of the plume, the shock in the saturation profile propagates upward. This shock-wave solution is followed by a rarefaction wave. The evolution of the bottom part of the plume is extremely slow at early times and is barely noticeable in the plots. Due to roundoff errors, numerical simulations may entirely miss it along with the following traveling wave (Riaz and Tchelepi, 2006). The slowness is a consequence of the water-wet environment where the permeability to water drops dramatically in the presence of gas. The high (relative to the gas) water viscosity further slows down the fluid exchange. Saturation S^0 at $\zeta = 0$ remains constant at this stage of plume evolution. The fluid displacement mechanism above $\zeta = 0$ is drainage, and it is imbibition for $\zeta < 0$.

When the main part of the plume collapses, the evolution of the bottom part of the saturation profile becomes faster, see Figure 2. Since the leading part of the saturation profile keeps on propagating with the same velocity, the traveling wave at the bottom compensates for the gas flow by propagating upward. Note that the speed of propagation of the bottom traveling wave exceeds V^*, given by Equation (15).

This second stage of plume evolution remains viable until the part of the saturation profile between the top and bottom traveling shock waves collapses. Once this happens, the saturation along the entire plume is close to the residual gas saturation. The plume continues to thin through the rarefaction wave centered at the bottom, Figure 3. Since the saturation of water in this last stage exceeds S^* in the entire plume, the propagation of the top of the plume slows down dramatically. The theory suggests asymptotic convergence of the saturation profile to the residual gas saturation.

3.3 Evolution of a plume at a horizontal interface

The theory developed above is for an idealized homogeneous formation. In this section, we consider propagation of the leading top of the plume through a horizontal interface between two different rocks. The subscript index $_1$ denotes the formation below the interface, and the index $_2$ denotes the formation above the interface. Thus, ϕ_1 and k_1 characterize the porosity and permeability of the rock underneath the interface, and ϕ_2 and k_2 characterize the porosity and permeability of the rock above the interface. Let S_1 be the saturation at the leading front on the top of the plume before crossing the interface. The gas

Darcy velocity at this saturation is given by

$$u_1 = \frac{k_1(\varrho_w - \varrho_g)g}{\phi_1 \mu_w} f_1(S_1) \tag{17}$$

On both sides of the interface, Darcy velocity of gas must be the same:

$$\frac{k_1(\varrho_w - \varrho_g)g}{\phi_1 \mu_w} f_1(S_1) = \frac{k_2(\varrho_w - \varrho_g)g}{\phi_2 \mu_w} f_2(S_2) \tag{18}$$

The fluid densities and viscosities cancel, so the last equation relates water saturations on both sides of the interface to the variation of rock properties.

Let a superscript asterisk * denote the saturation corresponding to the maximum velocity of propagation of the top front of the plume, and a superscript ^{M} denote the maximum of the fractional flow function:

$$\frac{f_i(S_i^*)}{1 - S_i^*} = \max_S \frac{f_i(S)}{1 - S}, \quad f_i(S_i^M) = \max_S f_i(S), \quad i = 1, 2 \tag{19}$$

In mass balance equation (18), S_1 is the saturation at the top of propagating plume. In a homogeneous medium, $S_1 = S_1^*$. It may be not so if a plume crosses an interface.

First, let us consider a case where no saturation S_2 can satisfy mass balance equation (18). This happens when the permeability of Medium 2 is insufficient to support gas flow in Medium 1. Therefore, gas saturation will start growing at the interface and the flow rate will slow down correspondingly. The brine saturation in Medium 1 at the boundary will reach some value S_1', which is less or equal to S_1^*, so that the Darcy velocity in Medium 1 will match the maximum Darcy velocity in Medium 2:

$$\frac{k_1}{\phi_1} f_1(S_1') = \frac{k_2}{\phi_2} f_2(S_2^*) \tag{20}$$

Here, we have cancelled similar terms from Equation (18). We are interested

in the smaller of the two saturations, S_1', satisfying Equation (20). Gas accumulation at the interface generates two shock waves on the saturation profile: an upward wave in Medium 2 with the velocity of propagation

$$v_2^* = \frac{k_2(\varrho_w - \varrho_g)g}{\phi_2 \mu_w} \frac{f_2(S_2^*)}{1 - S_2^*} \tag{21}$$

and a shock wave in Medium 1 with the velocity of propagation

$$v_1' = -\frac{k_1(\varrho_w - \varrho_g)g}{\phi_1 \mu_w} \frac{f_1(S_1^*) - f_1(S_1')}{S_1^* - S_1'} \tag{22}$$

Saturation S_1' is less than S_1^* due to gas accumulation. Since this gas accumulation reduces the Darcy velocity in order to equalize it with the fluid flow above the interface in Medium 2, one has $f_1(S_1') < f_1(S_1^*)$. The velocity v_1' is negative and the shock wave propagates downward, Figure 4.

Now, let the saturation S_1 be such that there exists a feasible saturation S_2, which satisfies Equation (18). Then, unless $S_2 = S_2^*$, two different saturations S_2 satisfy Equation (18). Since the plume propagates into a fully brine-saturated formation, only the larger solution is physically sensible. If saturation S_2 obtained from Equation (18) does not exceed S_2^*, $S_2 \leq S_2^*$, the gas supply from Medium 1 is sufficient to support the maximum velocity of plume propagation in Medium 2. In such a case, the plume propagates into Medium 2 with the theoretically maximal velocity described by Equation (21). The leading shock wave is followed by a rarefaction wave. The latter may or may not extend all the way to the stable point of maximal Darcy velocity, that is to the saturation S_2^M, Figure 5.

If the arriving plume is so lean with respect to gas that the brine saturation S_2 obtained from the continuity equation (18) exceeds S_2^*, then the velocity

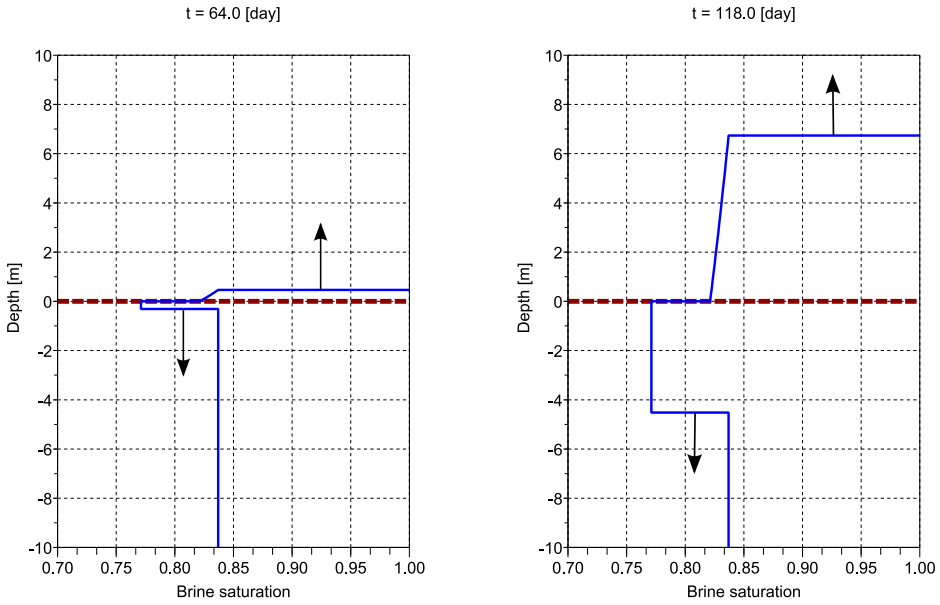

Fig. 4. A plume crossing the boundary: the permeability of the formation above the interface is 100 mD, which is less than the permeability of 151 mD of the formation beneath the boundary (bold dashed line). The porosities are, respectively, equal to 0.20 and 0.23. Accumulation of gas beneath the boundary generates a shock wave traveling downward. The arrows show the directions of propagation of the fronts.

of plume propagation in Medium 2 is

$$v_2 = \frac{k_2(\varrho_w - \varrho_g)g}{\phi_2 \mu_w} \frac{f_2(S_2)}{1 - S_2} < v_2^* \tag{23}$$

Figure 6 shows propagation of a lean plume.

3.4 Plume propagation in a heterogeneous formation

Let us consider a formation of thickness H subdivided into zones with different properties. Inside each zone, the formation is assumed to be homogeneous. Let N be the total number of zones and H_i be the thickness of layer i, numbered in the direction of the plume propagation: from the bottom to the top. To

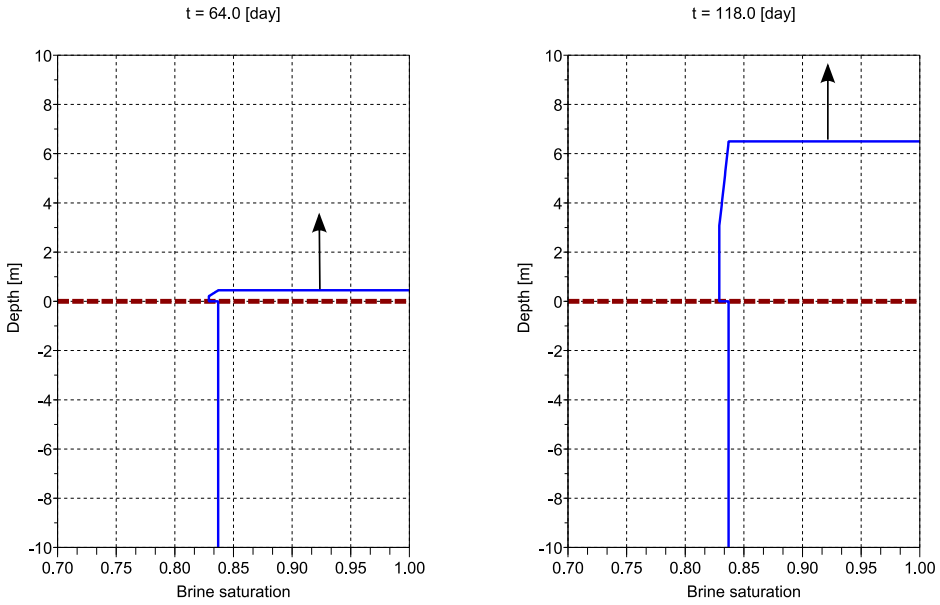

Fig. 5. A plume crossing the boundary: the formation permeability above the interface is 99 mD, which is only slightly less than 100 mD beneath the boundary (bold dashed line). The porosities are, respectively, 19% and 20%. The rarefaction wave behind the leading front transforms into constant-saturation flow.

evaluate the time of the plume crossing each layer, one needs to estimate the respective velocity v_i of the plume propagation. We obtain such an estimate using the results of the previous section.

In each layer, the velocity of plume propagation is either equal to the theoretical maximum, v_i^*, or is less than that if the underlying low-permeability layers reduce the actual velocity to a lower value. In the first case, the time of crossing the layer can be estimated upfront:

$$\tau_i^* = \frac{H_i}{v_i^*} = \frac{\phi_i \mu_w H_i}{k_i(\varrho_w - \varrho_g)g} \frac{1 - S_i^*}{f_i(S_i^*)} \tag{24}$$

If the maximal velocity of propagation is possible in all sublayers, the total

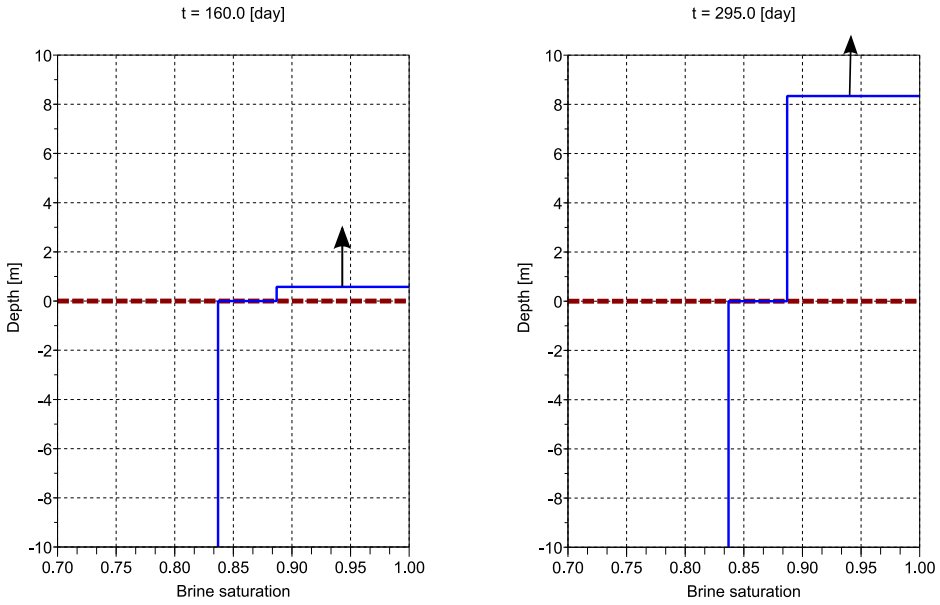

Fig. 6. Lean plume behind the boundary: the gas supply below the boundary (bold line) is insufficient to support the maximum velocity of propagation above the boundary. The permeability and porosity above the interface are 100 mD and 20%. Under the interface, the permeability and porosity are lower: 20 mD and 12%. The time elapsed between the shown saturation profiles is one month. The arrow shows the direction of propagation of the front.

time, T^*, is determined by summation

$$T^* = \sum_i \frac{\phi_i \mu_w H_i}{k_i(\varrho_w - \varrho_g)g} \frac{1 - S_i^*}{f_i(S_i^*)} \tag{25}$$

This is the theoretical minimum of plume propagation time.

Now, let us consider a case where in some layers the maximal velocity of propagation may be unattainable. In such a case, in each layer the saturation at the top front of the plume must be calculated by a sequential solution of equation (18) from the bottom layer to the top. In particular,

$$f_i(S_i) = \frac{k_i \phi_{i-1}}{k_{i-1} \phi_i} f_{i-1}(S_{i-1}) \tag{26}$$

The time of crossing of the layer i is equal to

$$\tau_i = \frac{\phi_i \mu_w H_i}{k_i(\varrho_w - \varrho_g)g} \frac{1 - S_i}{f_i(S_i)} \tag{27}$$

Repeatedly applying equation (26), one gets

$$f_i(S_i) = \frac{k_i}{\phi_i} \frac{\phi_1}{k_1} f_1(S_1) \tag{28}$$

After substitution of this result into Equation (27) and summation in i, the total travel time is

$$T = \frac{\mu_w}{(\varrho_w - \varrho_g)g} \frac{\phi_1}{k_1} \frac{1}{f_1(S_1)} (1 - \overline{S}) H \tag{29}$$

where $\overline{S}$ is the mean brine saturation:

$$\overline{S} = \sum_i S_i \frac{H_i}{H} \tag{30}$$

Equation (29) relates the mean velocity of propagation of the plume in a heterogeneous formation, $\overline{v}$, to the mean brine saturation

$$\overline{v} = \frac{k_1(\varrho_w - \varrho_g)g}{\phi_1 \mu_w} \frac{f_1(S_1)}{1 - \overline{S}} \tag{31}$$

If the permeability and porosity distributions $k(z)$ and $\phi(z)$ are known, and the dimensionless fractional flow function does not depend on depth, then, in case of a sub-maximal plume propagation velocity, the saturation distribution can be predicted from Equation (28):

$$S(z) = f^{-1}\left(\frac{k(z)}{\phi(z)} \frac{\phi_1}{k_1} f(S_1)\right) \tag{32}$$

This equation leads to an estimate of the mean saturation at the leading front of the plume and, respectively, to an estimate of the plume travel time.

3.5 The impact of heterogeneity on plume propagation time

Let us assume that the relative permeability curves are the same for the rock above and below the interface, so that one can use the same fractional flow function, $f(S)$. Then, the water saturation at the leading front of the plume is always equal or exceeds S^*. Calculations in the previous section suggest the following rule for estimating the velocity of propagation when the plume crosses an interface between two media. If

$$f(S^*) \leq \frac{k_1\phi_2}{k_2\phi_1} f(S_1) \tag{33}$$

then $S_2 = S^*$ and the plume front propagation speed in Medium 2 is at maximum. If the opposite inequality holds true, then S_2 must be determined from Equation (20), and Equation (23) determines the velocity of plume propagation. This calculation must be repeated for all layers from the bottom to the top.

For illustration, consider a layered formation with a random permeability distribution, see Figure 7. Figure 8 shows plume propagation as a function of time, accounting for the variations in permeability and ignoring it by using the harmonic mean permeability of all layers as an effective uniform permeability. This example shows that heterogeneous layers slow down plume propagation. The nature of this phenomenon is in the nonlinear dependence of the flow on fluid saturation. As a consequence, the saturation in a high-permeability layer overlaying a low-permeability layer can be different from the saturation S^*.

To quantify the impact of heterogeneity on the time of plume propagation, a number of simulations has been run for various realizations of random distribution of the absolute permeability. The aquifer in this example consists

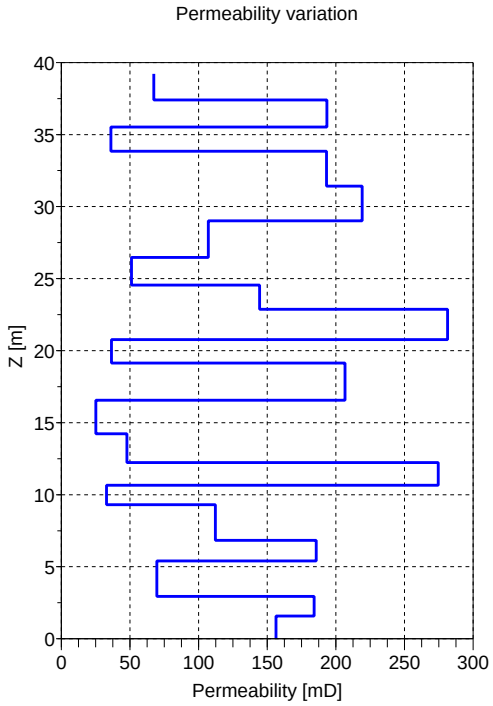

Fig. 7. Vertical permeability profile.

of 20 equally-thick layers of different permeabilities. Each layer is 2-meters thick. The standard deviation of the permeability scaled by the harmonic mean quantifies the heterogeneity of the formation. Similar to the example in Figure 8, two propagation times are evaluated for each realization. First, the propagation time is evaluated accounting for the heterogeneities as described earlier in this section. Second, the propagation time is predicted under the assumption that the entire aquifer is homogeneous and the effective permeability equals the harmonic mean of the layer permeabilities. The measure of delay is the ratio of the two times, which is a dimensionless quantity. Figure 9 shows the results obtained for 250 realizations. It shows a linear trend (solid line) of increasing time delay with increasing heterogeneity.

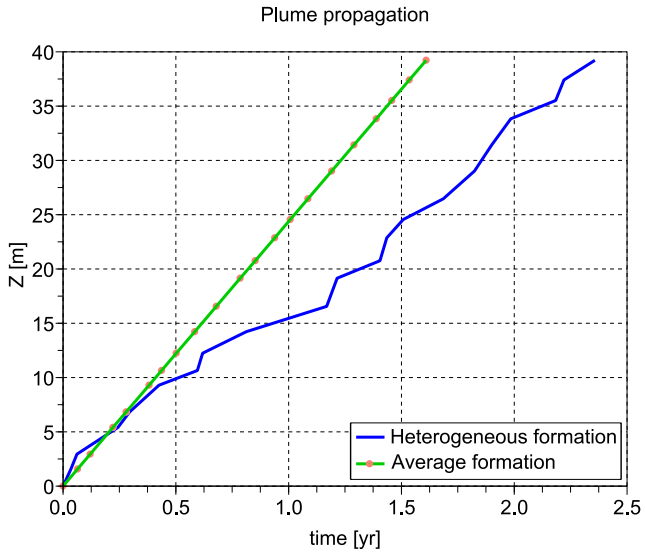

Fig. 8. Vertical plume propagation versus time. The straight line shows propagation in a homogeneous formation with the harmonic mean of permeability from the profile in Figure 7. The polygonal line has been calculated accounting for the heterogeneity. The dots are centered at the boundaries between the layers.

3.6 Dispersion of plume front velocity by heterogeneities

Consider a vertical cross-section of an aquifer with the dimensions and distribution of permeability shown in Figure 10. In this computer-generated medium, we apply the model of vertical flow developed above. The simulations involve a percolation-like algorithm accounting for the time of plume evolution. Our model neglects lateral flow, so the estimates and calculations are just a first approximation. The impact of lateral flow increases in a medium with correlated heterogeneities, like inclined permeable fractures. In an uncorrelated random medium, like the one in Figure 10, the horizontal component of the

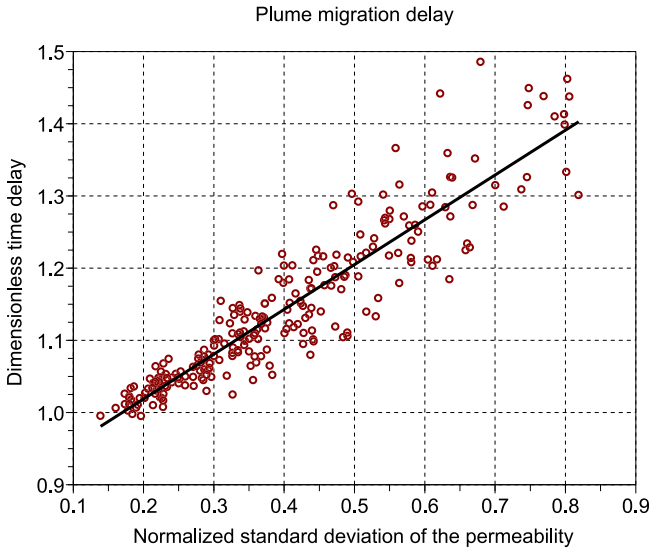

Fig. 9. Dimensionless plume delay versus normalized variance of permeability.

pressure gradient remains relatively small. Comprehensive 3D simulations require numerical approach and are beyond the scope of this study. Figure 11 shows the dispersion of the front of the plume caused by the heterogeneity. Although the plot in Figure 11 is based on a one-dimensional model, it is in agreement with the conclusions of Bryant et al. (2006), which are based on a series of numerical simulations in two dimensions. Namely, the dispersion of the front of the plume is a result of formation heterogeneity, rather than a consequence of intrinsic instabilities such as viscous fingering.

The result is significantly different if there is a permeable vertical conduit, like a crack, Figure 12. Figure 13 shows fast propagation of the plume inside the crack, whereas the character of front propagation in the rest of the plume is similar to that in Figure 11.

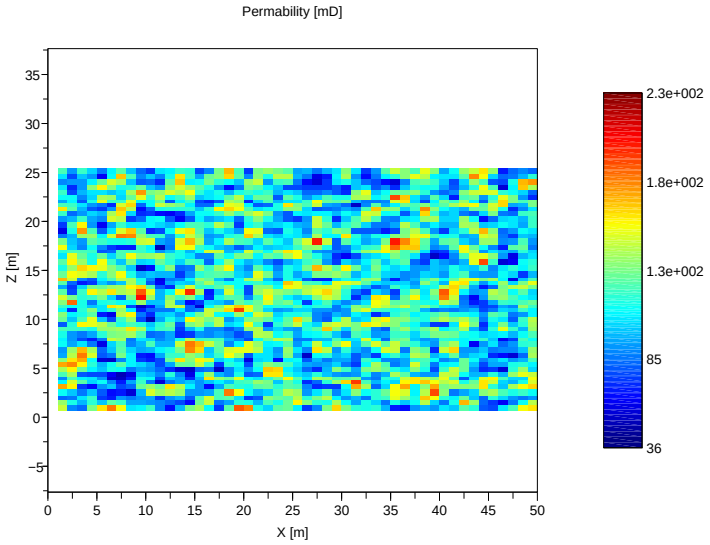

Fig. 10. A computer-generated vertical cross-section of uncorrelated heterogeneous formation.

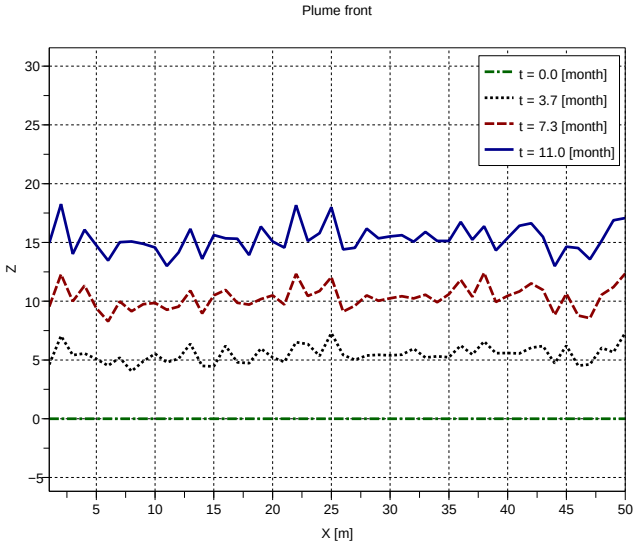

Fig. 11. Front propagation in formation shown in Figure 10.

4 Summary and conclusions

Buoyancy-driven viscous flow of a gas plume is modeled as one-dimensional two-phase countercurrent flow. This approximation is applicable to the flow

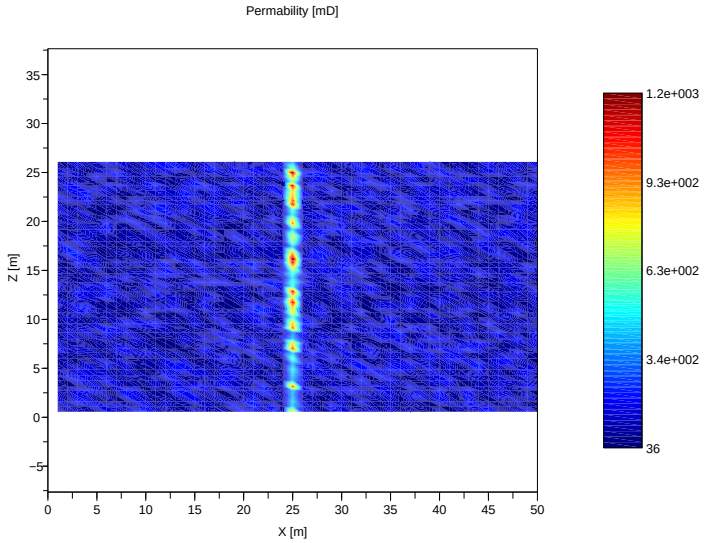

Fig. 12. A computer-generated vertical cross-section of heterogeneous formation with a permeable crack in the center.

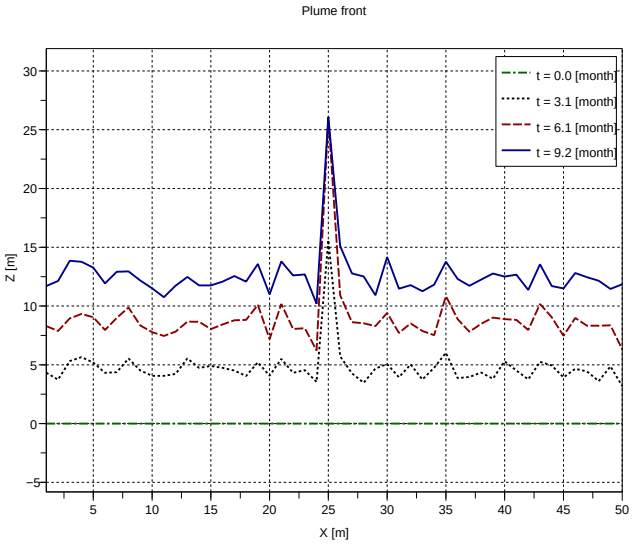

Fig. 13. Front propagation in a permeable vertical crack is much faster than in the rest of the plume.

far enough from the lateral boundaries of a plume, which is spread horizontally. In a vertical fracture or other laterally confined brine-saturated structure the flow also can be described as one-dimensional. Under certain conditions,

Equation (5), the capillary pressure can be neglected, which leads to a hyperbolic model of flow. The method of characteristics suggests two types of solutions: shock and rarefaction waves. The theory predicts that in a porous medium, a laterraly spread gas plume does not migrate upward like a bubble in bulk water. Instead, the leading part of the plume, having a relatively low gas saturation propagates much faster than the main part of the plume, which stays almost stationary. The saturation at the leading front of the plume can be estimated from the dimensionless fractional flow function through a simple calculation.

The theory admits an extension to a heterogeneous aquifer. For a simple model of layered formation, it suggests rules of plume flow across an interface between two adjacent layers with different rock properties. Iteration of this rule leads to a prediction of the evolution of gas plume in a layered reservoir. The principal conclusion is that a layered heterogeneity slows down propagation of the plume. Therefore, estimates based on a homogeneous medium with effective permeability can be wrong. The reason of the slowing-down impact of heterogeneity is that a single low-permeability layer dramatically reduces the plume propagation velocity in all overlaying strata. Statistical analysis of evaluation of plume travel time delay due to heterogeneity leads to a linearly increasing trend of this delay relative the standard deviation of the permeability distribution between the layers. Field and experimental work will help to scale and calibrate the most important parameters.

The one-dimensional model of countercurrent vertical vertical flow presented here yields exact solutions free of truncation errors and numerical dispersion. The formulae explicitly express propagation velocity of the plume front through the properties of the fluids and formation. We believe that the theory

developed here provides reasonable estimates of the time of plume propagation from the formation flow properties in case of uncorrelated heterogeneities. The model remains applicable when the formation includes a permeable vertical crack. In such a case, even if the mean permeability of the latter only slightly exceeds that of the rest of the domain, calculations predict that the plume propagation inside the crack is much faster than in the other regions of the formation. However, if the formation includes correlated inconformities, which are not vertically oriented, then the lateral component of the flow vector cannot be neglected, which makes the model presented here insufficient. A comprehensive analysis of gas plume migration in a heterogeneous formation in two or three dimensions may require numerical simulations (Bryant et al., 2006; Riaz and Tchelepi, 2006). Two-dimensional simulations reported by Bryant et al. (2006) show that dispersion of the front of the plume is associated with lateral heterogeneity of the medium rather than development of dynamic instabilities such as viscous fingers.

5 Recommendations

The character of evolution of the vertical saturation profile implied by the theory developed here suggests that in a homogeneous reservoir a laterally-distributed plume should spread over the overlaying formation. To maximize the volume of trapped gas, it seems attractive to inject it at the bottom part of a permeable aquifer in such a way that during injection the injected gas spreads out laterally as much as possible. Such injection pattern can be achieved by a injection via a horizontal and/or multilateral well.

Acknowledgments

This work was supported by the U.S. Department of Energy's Assistant Secretary for Coal through the Zero Emission Research and Technology Program under US Department of Energy contract no. DE-AC02-05CH11231 to Lawrence Berkeley National Laboratory (LBNL). The authors a grateful to Dr. Andrea Cortis and Dr. Stefan Finsterle of LBNL for reviewing the manuscript and suggesting numerous improvements. We also thank the anonymous reviewers for critical remarks and suggestions.

References

Al-Futaisi, A., Patzek, T. W., 2003. Impact of wettability on two-phase flow characteristics of sedimentary rock: Quasi-static model. Water Resources Research 39 (2), 1042–1055.

Bedrikovetsky, P., De Deus, J., Altoé, J. E., 2001. Secondary migration of oil: Analytical model. SPE 69411. In: 2001 SPE Latin American and Carribean Petroleum Engineering Conference. SPE, Buenos Aires, Argentina.

Bryant, S. L., Lakshminarasimhan, S., Pope, G. A., 2006. Buoyancy dominated multiphase flow and its impact on geological sequestration of CO_2, SPE 99938. In: 2006 SPE/DOE Symposium on Improved Oil Recovery 2226 April 2006. SPE, Tulsa, OK.

Buckley, S. E., Leverett, M. C., 1942. Mechanisms of fluid displacement in sands. Trans. AIME 146, 149–158.

Hubbert, M. K., 1956. Darcy's law and the field equations of the flow of underground fluids. Trans. AIME 207 (7), 222–239.

Juanes, R., Spiteri, E. L., Orr Jr., F. M., Blunt, M. J., 2006. Impact of relative

permeability hysteresis on geologic CO_2 storage. Water Resources Research 42, W12418, doi:10.1029/2005WR004806.

Landau, L. D., Lifshitz, E. M., 1959. Course of Theoretical Physics. Fluid Mechanics. Vol. 6 of Series in advanced physics. Addison-Wesley, Reading, Mass.

Lax, P., 1973. Hyperbolic Systems of Conservation Laws and the Mathematical Theory of Shock Waves. Society of Industrial and Applied Mathematics, Philadelphia.

Leverett, M. C., Lewis, W. B., True, M. E., 1942. Dimensional-model studies of oil-field behavior. Trans. AIME 146, 175–193.

Luan, Z.-A., 1994. Some theoretical aspects of gravity drainage in naturally fractured reservoirs, SPE 28641. In: 69th SPE Annual Technical Conference and Exhibition. SPE, New Orleans, LA, pp. 357–366.

Muskat, M., 1949. Physical Principles of Oil Production. McGraw-Hill, New York, NY.

Petrovskii, I. G., 1966. Ordinary differential equations. Prentice-Hall, Englewood Cliffs, NJ.

Riaz, A., Tchelepi, H. A., 2006. Dynamics of vertical displacement in porous media associated with CO_2 sequestration. SPE paper 103169. In: 2006 SPE Annual Technical Conference and Exhibition. September 24–27, 2006. SPE, San Antonio, TX.

Siddique, F. I., Lake, L. W., 1997. A comprehensive dynamic theory of hydrocarbon migration and trapping. SPE 38682. In: 1997 72^{th} Annual Technical Conference and Exhibition. SPE, San Antonio, TX.

Silin, D., Patzek, T. W., Benson, S. M., September 2006. Exact solutions in a model of vertical gas migration. SPE paper 103156. In: 2006 SPE Annual Technical Conference and Exhibition. September 24–27, 2006. SPE, San

Antonio, TX.

Silin, D., Patzek, T. W., Benson, S. M., 2007. A model of buoyancy-driven two-phase countercurrent fluid flow. Laboratory report LBNL-62607, Lawrence Berkeley National Laboratory, Berkeley, CA.

Valvante, P. H., Blunt, M. J., 2004. Predictive pore-scale modeling of two-phase flow in mixed-wet media. Water Resources Research 40, W07406, doi:10.1029/2003WR002627.

Xu, T., Apps, J. A., Pruess, K., April 2005. Mineral sequestration of carbon dixoide in. a sandstone-shale system. Chemical Geology 217 (3-4), 295–318.